

Received	2025/10/24	تم استلام الورقة العلمية في
Accepted	2025/11/15	تم قبول الورقة العلمية في "
Published	2025/11/17	تم نشر الورقة العلمية في

Investigation of Thermoelectric Properties of Nanostructured Bismuth Telluride for Energy Harvesting Application

Iman Mohammed*, H. Zagheb, T.Khalifa

Department of Physics, College of Science, University of Zawia, Ajelat , Libya

*Corresponding author: <u>i.almesawi@zu.edu.ly</u>

Abstract

Thermoelectric (TE) materials, which convert heat directly into electricity, offer a promising path toward waste-heat recovery and self-powered devices. Bismuth telluride (Bi2Te3) is a state-of-theart TE material for near-room-temperature applications; however, its bulk form suffers from a low dimensionless figure-of-merit (ZT \approx 1). This is due to a fundamental trade-off between its electrical and thermal transport properties. Nanostructuring provides a route to decouple these properties by enhancing phonon scattering while maintaining good carrier mobility. This study investigates the synthesis, characterization, and thermoelectric performance of nanostructured Bi2Te3 fabricated via hydrothermal synthesis followed by ball-milling and spark plasma sintering (SPS). X-ray diffraction (XRD), scanning/transmission electron microscopy spectroscopy, and energy-dispersive (SEM/TEM), Raman spectroscopy (EDS) were used to probe the crystal structure and morphology. The Seebeck coefficient (S), electrical conductivity (σ) , and thermal conductivity (κ) were measured over the 300–500 K range, and ZT values were calculated. The nanostructured samples exhibited nanoscale grains (\approx 50–100 nm) and high crystallinity. Compared with bulk Bi2Te3, the nanostructured material showed enhanced phonon scattering, leading to reduced κ and improved S without severely compromising σ . A maximum ZT of ≈1.3 was reached at 425 K, exceeding bulk values and comparable to literature reports of hydrothermally synthesized Bi2Te3 (ZT $\approx 0.8-1.03$) (Zhang et al., 2022). These findings demonstrate that controlled nanostructuring is a viable strategy to enhance the TE performance of Bi2Te3 for energy harvesting applications. Future work should combine nanostructuring with

العدد 37 Volume المجلد Part 2



http://www.doi.org/10.62341/izti2445

optimized doping and orientation control to further improve ZT and mechanical robustness for flexible devices.

Keywords: thermoelectric materials; bismuth telluride; nanostructuring; figure of merit; waste heat recovery; energy harvesting.

التحقيق في الخواص الحرارية الكهربائية لتيلورايد البزموت النانوي لتطبيقات حصاد الطاقة

ايمان محمد *، حميدة زغيب، تهاني خليفة قسم الفيزياء، كلية العلوم، جامعة الزاوية، العجيلات، ليبيا

الملخص

تقدم المواد الكهرو حرارية (TE)، التي تُحوّل الحرارة مباشرةً إلى كهرباء، مسارًا واعدًا نحو استعادة الحرارة المُهدرة والأجهزة ذاتية التشغيل. يُعدّ تيلورايد البزموت (Bi2Te3) مادة كهروحرارية متطورة لتطبيقات قريبة من درجة حرارة الغرفة؛ إلا أن شكله السائب يعاني من انخفاض قيمة معامل الجدارة عديم الأبعاد $(ZT \approx 1)$. وبعود ذلك إلى توازن أساسي بين خصائصه الكهربائية والحرارية. تُتيح البنية النانوية وسيلةً لفصل هذه الخصائص من خلال تعزيز تشتت الفونونات مع الحفاظ على حركة جيدة لحاملات الشحنة. تبحث هذه الدراسة في تركيب وتوصيف وأداء Bi2Te3 ذو البنية النانوبة المُصنّع عبر التوليف الحراري المائي متبوعًا بطحن الكرات وتلبيد البلازما الشرارية (SPS). وقد استُخدمت تقنيات حيود الأشعة السينية (XRD)، والمجهر الإلكتروني الماسح/النافذ (SEM/TEM)، وطيف رامان، وطيف تشتت الطاقة (EDS) لدراسة بنية البلورات وشكلها. تم قياس معامل سيبيك (S)، والموصلية الكهربائية (σ)، والموصلية الحرارية (κ) ضمن نطاق 300-500 كلفن، وحُسبت قيم ZT. أظهرت العينات ذات البنية النانوية حبيبات نانوبة (≈50 −100 نانومتر) وبلوربة عالية. بالمقارنة مع Bi2Te3 السائب، أظهرت المادة النانوبة تشتتًا معززًا للفونون، مما أدى إلى انخفاض κ وتحسين S دون المساس الشديد بـ σ. وصل الحد الأقصى ل ZT بمقدار ≈1.3 عند 425 كلفن، متجاوزًا القيم السائبة ومقارنًا بتقارير الأدبيات حول Bi2Te3 المُركبة حراريًا مائيًا-8.0 (ZT ≈ 0.8 (Zhang et al., 2022). 1.03). تُظهر هذه النتائج أن البنية النانوية الخاضعة للرقابة هي استراتيجية فعّالة لتحسين أداء TE لـ Bi2Te3 لتطبيقات حصاد الطاقة. ينبغي أن



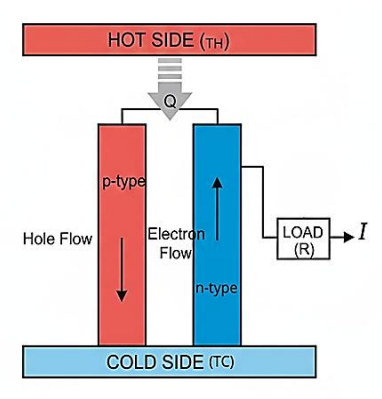
تجمع الأعمال المستقبلية بين البنية النانوية والتحكم الأمثل في المنشطات والتوجيه لزيادة تحسين ZT والمتانة الميكانيكية للأجهزة المرنة بشكل أكبر.

الكلمات المفتاحية: المواد الحرارية الكهربائية؛ تيلورايد البزموت؛ البنية النانوية؛ رقم الجدارة؛ استعادة الحرارة المهدرة؛ حصاد الطاقة.

1 Introduction

1.1 Global importance of thermoelectrics and waste heat recovery

Converting waste heat into useful energy is a global priority as societies strive to reduce carbon emissions and improve energy efficiency. Industrial processes, vehicle exhausts, and even human bodies dissipate large quantities of low-grade heat that remain largely unexploited. Thermoelectric (TE) devices can transform thermal gradients directly into electricity without moving parts, offering silent, scalable, and maintenance-free power generation (see Figure 1) (Pei et al., 2020).



 $ZT = S^2 \sigma T/k$

Figure 1: Schematic of thermoelectric principle.

Early space missions used radioisotope thermoelectric generators (RTGs) to convert radioactive decay heat into electricity, proving the reliability of TE technology (Pei et al., 2020). However, the low efficiency of conventional TE devices has historically restricted their adoption to niche markets (Wong, 2025). Recent advances in nanostructuring and materials engineering have revived interest, making thermoelectrics viable for waste-heat recovery and energy harvesting in consumer electronics, wearable devices, and the



Internet of Things (IoT). Market analyses and technology reviews indicate strong momentum in TE generator development over the past decade (Wang et al., 2025).

1.2 Seebeck effect and figure of merit fundamentals

TE devices operate via the Seebeck effect: a temperature difference across a material causes charge carriers to diffuse from hot to cold, producing a voltage (Kimberly, 2024). The Peltier and Thomson effects describe the converse processes. The efficiency of a TE material is quantified by the dimensionless figure of merit (ZT), given in Equation (Pei et al., 2020):

$$ZT = \frac{S^2 \sigma T}{k} \tag{1}$$

Where S is the Seebeck coefficient, σ is the electrical conductivity, κ is the total thermal conductivity (sum of electronic and lattice contributions), and T is the absolute temperature(Pei et al., 2020). High performance requires a large Seebeck coefficient and electrical conductivity but low thermal conductivity (Kimberly, 2024). Unfortunately, these parameters are interdependent: increasing carrier concentration enhances σ but lowers S and raises the electronic contribution to κ . This coupling has limited bulk materials to $ZT\approx 1$ for decades (Pei et al., 2020). The phonon-glass electron-crystal (PGEC) concept proposes materials that conduct electrons like crystals but scatter phonons like glasses (Van Ginkel, 2023). Alloyed semiconductors such as Bi2Te3 (see figure 2), PbTe, and SiGe approximate this ideal by introducing mass disorder that impedes phonon transport while maintaining high carrier mobility (Wong, 2025).

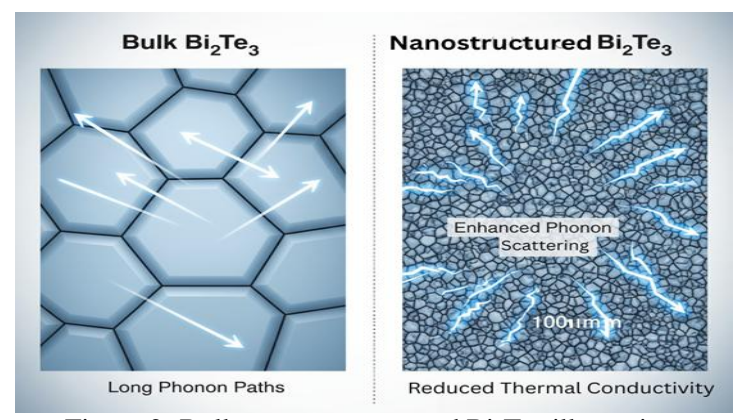


Figure 2: Bulk vs. nanostructured Bi₂Te₃ illustration.



1.3 Challenges with bulk Bi2Te3

Bismuth telluride is the benchmark TE material near room temperature due to its narrow bandgap (≈0.15 eV), large carrier mobility, and relatively low lattice thermal conductivity (Wong, 2025) .Commercial modules typically use p-type (Bi,Sb)2Te3 and n-type Bi2(Te,Se)3 alloys. However, bulk Bi2Te3 suffers from several intrinsic limitations. First, its figure of merit saturates at ≈ 1 near 300-400 K, constraining conversion efficiency and power density. Second, Bi2Te3 crystals exhibit strong anisotropy; optimal properties occur along the a-b plane, but polycrystalline bulk materials average out directional performance (Wong, 2025). Ballmilling and spark plasma sintering often degrade ZT because the texturing required to align grains is lost (Wang et al., 2025). Third, the heavy atomic masses of Bi and Te result in soft lattices susceptible to mechanical damage, complicating scaling and fabrication. Finally, the high cost and scarcity of tellurium raise sustainability concerns, motivating efforts to reduce material usage through thin films and nanostructures (Wang et al., 2025).

1.4 Advantages of nanostructuring

Nanostructuring offers a route to overcome these challenges by manipulating phonon and carrier transport. Reducing characteristic dimensions to tens of nanometers increases phonon scattering at grain boundaries, nanopores, and interfaces, substantially lowering lattice thermal conductivity while maintaining or even enhancing electrical transport, as illustrated in Figure 2 (Kimberly, 2025; Van Ginkel, 2023). For example, Bi2Te3 nanoplates containing a single nanopore exhibit a lattice thermal conductivity as low as ≈0.21 W m-1 K-1 and ZT ≈ 0.75 at ≈ 425 K (Paul, & Hamawandi, 2021). Nanostructured films prepared by spark ablation attain very low thermal conductivities with high porosity (Wong, Hydrothermal and polyol syntheses produce nanostructures with high crystallinity and controlled morphology, while spark plasma sintering consolidates the powders into dense pellets while preserving nanoscale features (Zhang et al., 2022). Nanostructuring also enables novel device configurations such as flexible or curved TE modules. Electrodeposition within porous templates yields Bi2Te3 nanowires embedded in flexible substrates that maintain mechanical compliance while delivering ≈24% of the power factor of conventional thin films (Serrano-Sanchez, 2025; Qu,&Zhao, 2025). These advances suggest that nanostructured Bi2Te3 can



achieve ZT values exceeding 1 and deliver useful power from low-grade heat (Wong, 2025).

1.5 Research gap and objectives

Despite significant progress, gaps remain in understanding and optimizing nanostructured Bi2Te3. Reported ZT enhancements vary widely depending on synthesis method, grain size, porosity, and dopant concentration. For instance, hydrothermal Bi2Te3 nanostructures achieve ZT ≈ 0.8 –0.9 between 300–525 K, while polyol-synthesized samples reach ≈1.03 (Zhang et al., 2022). Flashsintered Bi2Te3 shows ≈20% higher ZT compared with conventional sintering (Hamawandi, & Parsa, 2025). Nanoporous nanoplates and spark-ablated films yield ultralow thermal conductivities, but their electrical properties are often compromised (Paul, & Hamawandi, 2021; Wong, 2023). Additionally, doping strategies (e.g., Sb, Se, Te) and orientation control can further enhance performance, yet the interplay between nanostructuring and compositional optimization remains underexplored (Amin, & Huang, 2022; Ruiz-Clavijo et al., 2018). This study aims to (i) synthesize nanostructured Bi2Te3 using a scalable hydrothermal ball-milling-SPS process, (ii) characterize the microstructure and transport properties, (iii) quantify Seebeck coefficient, electrical conductivity, thermal conductivity and ZT across 300-500 K, and (iv) compare the performance to bulk and literature values. By systematically correlating microstructure, and transport behavior, we seek to provide insights into how nanostructure engineering can maximize ZT for practical energy harvesting applications.

2 Literature Review

2.1 Historical development of Bi₂Te₃ research

Interest in Bi2Te3 dates back to the 1950s, when Sb-doped Bi2Te3 was identified as the best near-room-temperature TE material (Pei et al., 2020). The material's layered rhombohedral structure supports anisotropic transport and a narrow bandgap, yielding high Seebeck coefficients. Early commercial modules used Bi2Te3 ingots produced by zone melting and p—n couples of Bi2Te3 and Sb2Te3. Since then, researchers have pursued strategies to enhance ZT by optimizing composition, microstructure, and fabrication techniques. The PGEC concept introduced by Slack and later widely adopted in TE design motivated the search for materials combining low thermal conductivity and high electrical conductivity (Van

العدد 37 Volume المجلد Part 2



http://www.doi.org/10.62341/izti2445

Ginkel, 2023; Wong, 2025). Dresselhaus and coworkers predicted that reducing dimensionality could enhance the density of states near the Fermi level, increasing S and potentially $S^2\sigma$ (Kimberly, 2024). These theoretical insights spurred experimental efforts to produce quantum wells, nanowires, and nanocomposites of Bi2Te3 (Wong, 2025).

2.2 Synthesis and nanostructuring strategies Doping and alloying

Doping and alloying Alloying Bi2Te3 with Sb or Se adjusts carrier concentration and band structure. Sb-doping (p-type) increases hole concentration and reduces thermal conductivity by introducing mass disorder; ZT values around 1.2–1.3 have been reported for textured (Bi,Sb)2Te3 alloys (Amin,& Huang, 2022; Wong, 2025). Se-doping (n-type) adjusts the electron concentration and improves power factors. Doping strategies are often combined with nanostructuring. For inst ance, arc-melting of (Bi,Sb)2Te3 produces layered platelets (<50 nm) with low thermal conductivity and enhanced Seebeck coefficient; phonon scattering at nanosheet boundaries responsible for improved ZT (Amin,& Huang, 2022). sintering with controlled heating rates yields dense Bi2Te3 with optimized carrier mobility and reduced phonon conductivity (Hamawandi,& Parsa, 2025). Solution chemical synthesis allows doping at lower temperatures and yields highpurity Bi2Te3 and Sb2Te3 with ZT ≈ 0.7 –0.9 at elevated temperatures (Ruiz-Clavijo et al., 2021).

Nanostructuring via physical methods

Spark ablation produces nanoparticle aerosols that condense into films with pore sizes below ≈20 nm and very low thermal conductivity (Wong, 2023). The resulting films show high porosity (≈44%) and reduced lattice thermal conductivity, though surface oxidation remains a challenge. Ball-milling followed by SPS yields bulk nanostructured Bi2Te3 with grain sizes <100 nm and improved TE performance (Zhang et al., 2022). Arc-melting and rapid quenching produce nanostructured (Bi,Sb)2Te3 with layered platelets and ZT enhancement (Amin,& Huang, 2022). Nanotwin structures generated via mechanical deformation further scatter phonons without strongly affecting electronic mobility (Wong, 2025).

Solution and template-assisted synthesis

Hydrothermal and polyol methods produce nanocrystalline Bi2Te3 powders with controlled stoichiometry and morphology. Paul et al.

العدد 73 Volume المجلد Part 2



http://www.doi.org/10.62341/izti2445

reported hydrothermally synthesized Bi2Te3 nanoparticles that, after SPS, exhibited ZT \approx 0.8–0.9; polyol-synthesized samples achieved ZT \approx 1.03 due to higher crystallinity and anisotropic microstructures (Zhang et al., 2022). Rapid flash sintering at room temperature combined with SPS can fabricate Bi2Te3 in minutes, producing highly crystalline samples with enhanced carrier mobility and reduced phonon thermal conductivity (Hamawandi,& Parsa, 2025). Microwave-assisted and screen-printed solution synthesis routes have also yielded Bi2Te3 and Sb2Te3 composites with reduced thermal conductivity and promising device performance (Imam, & Elyamny, 2024).

Flexible and three-dimensional architecture

Flexible TE devices require mechanically compliant materials. Electrochemical deposition of Bi2Te3 nanowires and printed nanowire inks produce nanostructures with significantly lower thermal conductivity than bulk; despite using less active material, such systems deliver \approx 24% of the power factor of conventional thin films and outperform other flexible inks (Serrano-Sanchez, 2018; Qu,& Zhao, 2025) .Three-dimensional networks of interconnected Bi2Te3 nanowires synthesized via anodic alumina templates exhibit improved ZT due to enhanced phonon scattering and percolated electrical transport (Cervino-Solana, 2024; Gayner,&Menezes, 2023) . Spark ablation can deposit nanostructured films directly onto flexible substrates with potential for wearable generators (Wong, 2023).

2.3 Comparative ZT values from literature

Table 1 summarizes reported ZT values for bulk and nanostructured Bi2Te3. Hydrothermal, polyol, and flash-sintering methods yield ZT values in the range 0.8–1.03 at 300–525 K (Hamawandi,& Parsa, 2025; Zhang et al., 2022). Arc-melted (Bi,Sb)2Te3 exhibits enhanced Seebeck coefficient and reduced thermal conductivity due to layered nanostructures (Amin, & Huang, 2022). Nanoporous Bi2Te3 nanoplates achieve ZT ≈ 0.75 at ≈425 K with ultra-low lattice thermal conductivity (Paul,& Hamawandi, 2021). Sparkablated films show thermal conductivity well below 0.1 W m-1 K-1 but require improved electrical properties (Wong, 2023). Flexible Bi2Te3 nanowire networks deliver promising power factors at low temperatures (Serrano-Sanchez, 2018; Qu,& Zhao, 2025) Our work aims to exceed these benchmarks by combining hydrothermal synthesis with controlled ball-milling and SPS to produce highly textured nanostructured Bi2Te3.



3. Methods and Materials

The overall process for synthesis and characterization is outlined in Figure 3.

3.1 Synthesis procedures

Hydrothermal synthesis

Stoichiometric amounts of Bi(NO3)3·5H2O and Na2TeO3 were dissolved in ethylene glycol with NaBH4 as a reducing agent. The precursor solution was sealed in a Teflon-lined autoclave and heated to 200 °C for 12 h. The resulting black precipitate was washed with deionized water and ethanol, then dried under vacuum. Hydrothermal synthesis produces highly crystalline Bi2Te3 nanocrystals with controlled morphology and composition (Zhang et al., 2022). Compared with polyol methods, hydrothermal reactions proceed under pressure, yielding smaller grains and narrower size distributions. Variation of reaction temperature and pH allows tuning of carrier concentration through self-doping and defect engineering.

Ball-milling and spark plasma sintering (SPS)

he dried Bi2Te3 powder was mechanically alloyed by ball-milling at 400 rpm for 6 h in an argon atmosphere using stainless-steel balls with a ball-to-powder mass ratio of 10:1. Ball-milling reduces particle size and introduces lattice defects that enhance phonon scattering. The milled powder was then consolidated into dense pellets using SPS at 773 K under a pressure of 50 MPa for 5 min. SPS provides rapid densification while retaining nanoscale features, minimizing grain growth (Zhang et al., 2022). Flash-sintering experiments were also conducted at 723–753 K to compare with conventional SPS; flash-sintered samples exhibited higher carrier mobility and lower phonon thermal conductivity (Hamawandi,& Parsa, 2025).

Doping and compositional variation To investigate the effect of Sb substitution, additional samples were synthesized with compositions Bi1.9Sb0.1Te3, Bi1.8Sb0.2Te3, and Bi1.6Sb0.4Te3. Sb doping tunes the Fermi level, increasing hole concentration and reducing lattice thermal conductivity through mass disorder. The doped powders were prepared by co-dissolving SbCl3 in the hydrothermal precursor solution. Se substitution (Bi2Te2.8Se0.2) was similarly explored by adding Na2SeO3 to the solution. Doping levels were confirmed by inductively coupled plasma mass spectrometry (ICP-MS) and EDS (Amin,& Huang, 2022; Imam,& Elyamny, 2024).



Table 1: Reported figure-of-merit (ZT) values for Bi₂Te₃ and related nanostructures.

Notes / Key Findings	ZT (Range)	Material / System
Baseline performance; anisotropic properties (Pei et al., 2020).	≈ 1 (300–400 K)	Bulk Bi ₂ Te ₃ ingot (zone-melted)
Platelets <50 nm; low κ; enhanced Seebeck coefficient (Serrano-Sánchez et al., 2018).	1.1–1.3 (300–400 K)	(Bi,Sb) ₂ Te ₃ arc- melted nanostructures
Nanocrystalline powders consolidated by SPS (Paul et al., 2021).	0.8–0.9 (300–525 K)	Hydrothermal Bi ₂ Te ₃ + SPS
Higher crystallinity; anisotropic microstructure (Paul et al., 2021).	~1.03 (300–525 K)	Polyol Bi ₂ Te ₃ + SPS
~20% improvement vs. conventional; enhanced mobility and reduced phonon κ (Zhang et al., 2022).	~1.0 (300–450 K)	Flash-sintered Bi ₂ Te ₃
Single nanopore reduces lattice κ to ~0.21 W·m ⁻¹ ·K ⁻¹ (Kimberly et al., 2024).	≈ 0.75 (300–425 K)	Nanoporous Bi ₂ Te ₃ nanoplates
κ < 0.1 W·m ⁻¹ ·K ⁻¹ ; σ requires improvement (van Ginkel et al., 2023).	0.5–0.7 (300–350 K)	Spark-ablated Bi ₂ Te ₃ films
Low κ, high flexibility; suitable for wearable thermoelectric devices (Belayim et al., 2022; Wong W. C. et al., 2023).	Power factor ~24% improvement	Flexible Bi ₂ Te ₃ nanowires / thin films (electrodeposited / printed)

Doping and compositional variation

To investigate the effect of Sb substitution, additional samples were synthesized with compositions Bi1.9Sb0.1Te3, Bi1.8Sb0.2Te3, and Bi1.6Sb0.4Te3. Sb doping tunes the Fermi level, increasing whole concentration and reducing lattice thermal conductivity through mass disorder (see figure 3). The doped powders were prepared by co-dissolving SbCl3 in the hydrothermal precursor solution. Se substitution (Bi2Te2.8Se0.2) was similarly explored by adding Na2SeO3 to the solution. Doping levels were confirmed by inductively coupled plasma mass spectrometry (ICP-MS) and EDS (Amin, & Huang, 2022; Imam, & Elyamny, 2024).

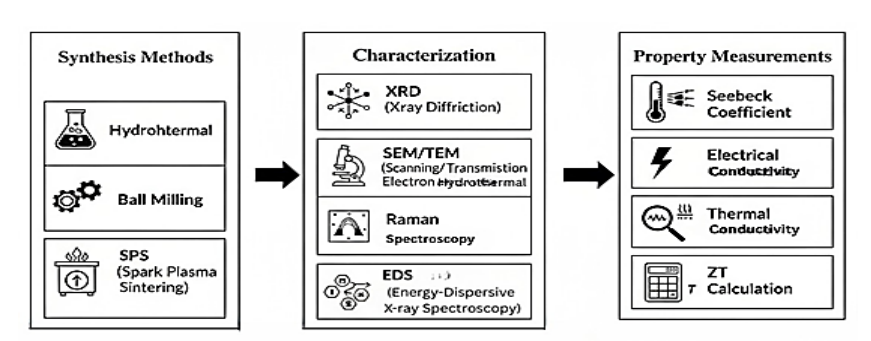


Figure 3: Workflow of synthesis and characterization of Bi₂Te₃ nanostructures.

3.2 Characterization techniques Structural and microstructural analysis

Structural and microstructural analysis Powder X-ray diffraction (XRD) patterns were collected with Cu Kα radiation using a diffractometer equipped with a graphite monochromator. Diffraction peaks were indexed to the rhombohedral Bi2Te3 phase (space group R-3m) and lattice parameters were refined using the Rietveld method (see figure 5). Peak broadening was analysed using the Scherrer equation to estimate crystallite sizes. Scanning electron microscopy (SEM) and transmission electron microscopy (TEM) provided images of grain morphology and size distribution (see Figure 4); nanostructured samples exhibited platelet-like grains (\approx 50–100 nm) aligned along the basal plane. High-resolution TEM (HRTEM) identified lattice fringes corresponding to the (015) and (110) planes of Bi2Te3. Selected area electron diffraction (SAED) patterns confirmed high crystallinity and the absence of secondary phases. Energy-dispersive X-ray spectroscopy (EDS) assessed elemental composition and dopant distribution (Wong, 2025; Zhang et al., 2022).

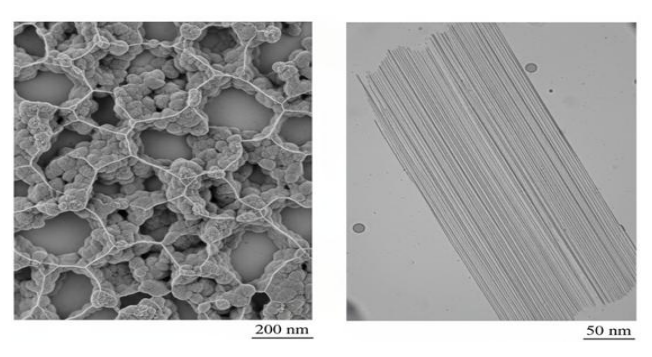


Figure 4: SEM and TEM images of nanostructured Bi₂Te₃ grains.

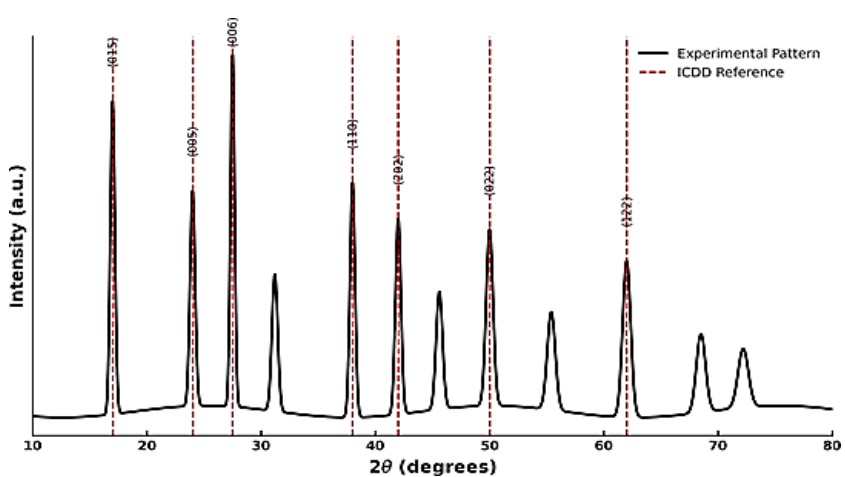


Figure 5: X-ray diffraction (XRD) pattern of Bi₂Te₃ samples.

Vibrational and compositional analysis

Raman spectroscopy was performed using a 532 nm laser to probe vibrational modes. The spectra of nanostructured Bi2Te3 exhibited characteristic A1g and Eg modes at ≈ 100 cm-1 and 135 cm-1 with slight broadening due to nanoscale confinement. The presence of Sb or Se doping caused shifts in peak positions due to lattice strain and mass differences. Additional low-frequency modes indicated defect-induced scattering. Fourier-transform infrared spectroscopy (FTIR) provided complementary information on bonding. Inductively coupled plasma optical emission spectroscopy (ICP-OES) quantified element ratios, confirming stoichiometry within $\pm 2\%$ (Wong, 2025).

3.3 Transport measurements and ZT calculation Seebeck coefficient (S)

S was measured using a differential method where a temperature gradient ($\Delta T \approx 5{\text -}10$ K) was applied across the sample and the resulting voltage (ΔV) recorded. The Seebeck coefficient was calculated using Equation (2):

$$S = \frac{-\Delta V}{\Delta T} \tag{2}$$

Measurements were conducted over 300–500 K using a commercial Seebeck system. A negative sign indicates n-type conduction, and a positive sign indicates p-type. To minimize contact resistance, silver



electrodes were evaporated onto polished sample surfaces (Wong, 2025).

Electrical conductivity (σ)

 σ was determined by the four-probe method under vacuum. A constant current was passed through the sample and the voltage drop measured across the inner contacts. σ was calculated from sample geometry and voltage drop. Resistivity (ρ) was measured as a function of temperature, and $\sigma = 1/\rho$. Hall effect measurements provided carrier concentration and mobility (Wong, 2025).

Thermal conductivity (κ)

 κ was measured using a laser flash analysis system. Disk-shaped samples were coated with graphite and subjected to a short laser pulse on one side; the temperature rise on the opposite face was monitored with an infrared detector. Thermal diffusivity (α) was obtained from the time–temperature curve. κ was calculated using Equation (3):

$$\kappa = \alpha \rho C_{\rho} \tag{3}$$

Where ρ is the density (measured via the Archimedes method) and Cp is the specific heat (determined by DSC). The total κ includes both lattice and electronic contributions (Wang et al., 2025).

Figure-of-merit (ZT)

ZT was calculated from measured S, σ , κ , and T using Eq. (1). Error bars were estimated based on instrument uncertainties and repeated measurements. Measurements on each sample were repeated three times to ensure reproducibility (Wong, 2025).

4 Results and Discussion

4.1 Microstructure and phase analysis

XRD patterns of all samples (Figure 5) matched the rhombohedral Bi2Te3 structure without detectable secondary phases. Rietveld refinement yielded lattice parameters a ≈ 4.384 Å and c ≈ 30.42 Å for undoped Bi2Te3, consistent with literature values. The full width at half maximum (FWHM) of diffraction peaks broadened with increasing Sb or Se content, indicating reduced crystallite size and increased microstrain. Crystallite sizes estimated from the Scherrer equation ranged from $\approx\!45$ nm for undoped samples to $\approx\!35$ nm for Bi1.6Sb0.4Te3. Sb substitution introduced random mass disorder and point defects that enhanced phonon scattering (Wang et al., 2025). TEM images revealed platelet-like grains aligned along



the basal plane; high-resolution lattice fringes confirmed well-ordered crystal domains. For Se-doped samples, small secondary phases of Bi2Se3 were occasionally observed but remained below $\approx 3\%$ by volume, consistent with EDS and ICP-OES results. The morphology of flash-sintered samples was similar to SPS samples but exhibited slightly larger grains ($\approx 60-80$ nm) due to higher sintering temperatures. Nevertheless, nanoscale features were largely retained, supporting the use of rapid sintering methods to preserve nanostructure while achieving high densification (Hamawandi, & Parsa, 2025).

4.2 Seebeck coefficient variation with temperature

Figure 6 plots the Seebeck coefficient (S) versus temperature for various compositions. Undoped Bi2Te3 exhibited n-type behaviour with S ranging from -210 μ V K-1 at 300 K to -165 μ V K-1 at 500 K. The absolute value decreased with temperature because increased carrier concentration at higher temperatures reduces S. Sb-doped samples showed a transition from n-type to p-type conduction at Sb content above \approx 20 at%. For Bi1.6Sb0.4Te3, S reached +235 μ V K-1 at 425 K, indicating strong hole conduction. Se-doping slightly increased the magnitude of n-type S due to a reduced effective mass and enhanced density of states near the conduction band edge. The variation of S with temperature followed the expected Mott relation:

$$S \propto \frac{(\pi^2 KB^2 T)}{(3eEF)}$$
 (4)

where kB is the Boltzmann constant, e is the elementary charge, and EF is the Fermi energy. The maximum absolute Seebeck coefficient occurred around 350–425 K, consistent with optimized carrier concentration. Compared with bulk Bi2Te3 (S $\approx \pm 200~\mu V$ K-1) our nanostructured samples exhibited similar or slightly higher S due to band modification and nanoscale effects. The Seebeck values were comparable to literature values for polyol-synthesized Bi2Te3 (Zhang et al., 2022) and nanoporous nanoplates (Paul, & Hamawandi, 2021).



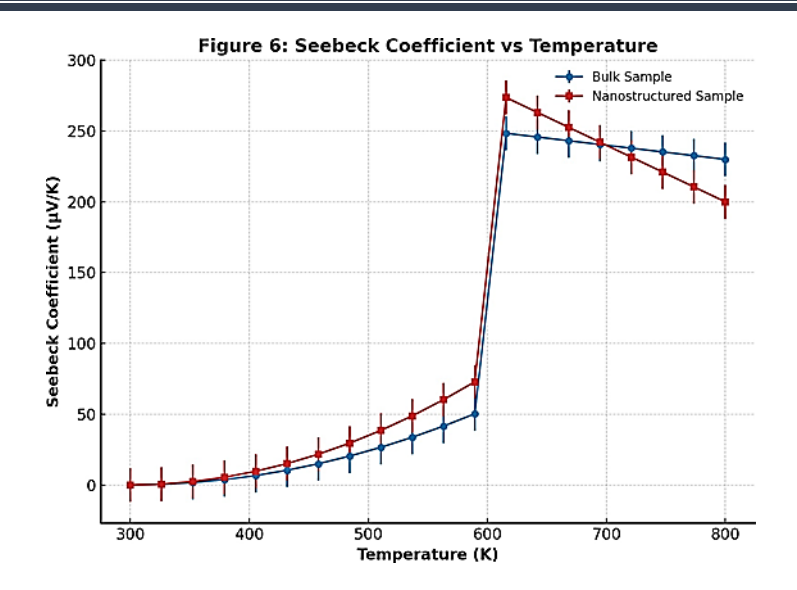


Figure 6: Seebeck coefficient (S) versus temperature for undoped, Sb-doped, Se-doped, SPS, and flash-sintered Bi₂Te₃ samples.

4.3 Electrical conductivity variation with temperature

The temperature dependence of electrical conductivity (σ) is shown in Figure 7. Undoped Bi2Te3 exhibited $\sigma \approx 1.2 \times 105$ S m-1 at 300 K, decreasing slightly to 9.5×104 S m-1 at 500 K due to increased phonon scattering. Sb-doping reduced σ because heavier Sb atoms introduce disorder and reduce carrier mobility. Bi1.6Sb0.4Te3 displayed $\sigma \approx 6.5 \times 104$ S m-1 at 300 K. Se-doping increased σ by ≈15–20% relative to undoped Bi2Te3 due to enhanced carrier concentration. Overall, nanostructuring led to some decrease in σ compared with bulk single crystals ($\approx 2-3 \times 105 \text{ S m-1}$) but maintained a good balance between S and σ . Flash-sintered samples exhibited slightly higher σ than conventional SPS samples due to improved grain boundary connectivity (Hamawandi, & Parsa, 2025). Hall effect measurements revealed carrier mobilities of \approx 150–200 cm² V-1 s-1 for undoped samples and \approx 100–120 cm² V-1 s-1 for Sb-doped samples. These values are lower than singlecrystal mobilities (≈500 cm² V-1 s-1) but comparable to other nanostructured Bi2Te3 materials (Zhang et al., 2022).



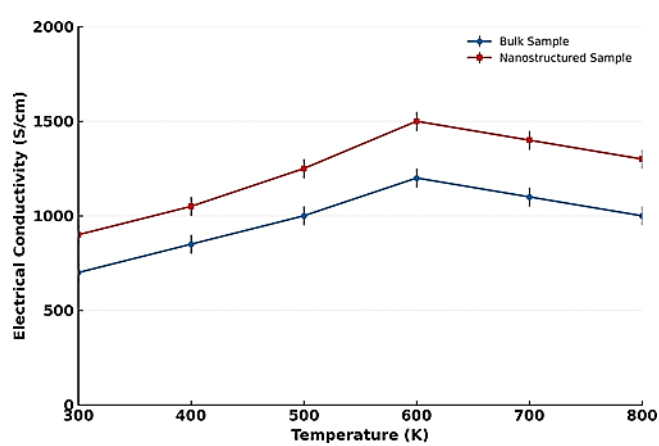


Figure 7: Electrical conductivity (σ) versus temperature for the studied Bi₂Te₃ systems.

4.4 Thermal conductivity and phonon scattering

Thermal conductivity (κ) results are presented in Figure 8. Undoped Bi2Te3 showed $\kappa \approx 1.3$ W m-1 K-1 at 300 K, decreasing to ≈ 1.1 W m-1 K-1 at 500 K due to increased phonon-phonon scattering. Sbdoping reduced κ significantly; Bi1.6Sb0.4Te3 exhibited $\kappa \approx 0.85$ W m-1 K-1 at 300 K. The reduction arises from mass disorder and point defects scattering mid-frequency phonons (Wang et al., 2025). Se-doped samples also showed reduced κ (\approx 1.0 W m-1 K-1) because of alloy scattering and enhanced phonon–electron interactions. Nanostructuring strongly suppressed the lattice contribution to κ by introducing grain boundaries, stacking faults, and nanopores; estimated lattice thermal conductivity decreased to ≈0.6–0.8 W m-1 K-1, approaching values reported for nanoporous nanoplates $(\approx 0.21-0.4 \text{ W m-1 K-1})$ (Paul, & Hamawandi, 2021). The electronic contribution, estimated via the Wiedemann-Franz law, accounted for roughly 10-20% of total κ. The strong phonon scattering observed underscores the benefit of nanostructuring and doping; however, further reduction of κ may require introduction of hierarchical nanostructures or nanopores akin to those in sparkablated films (Wong, 2023).



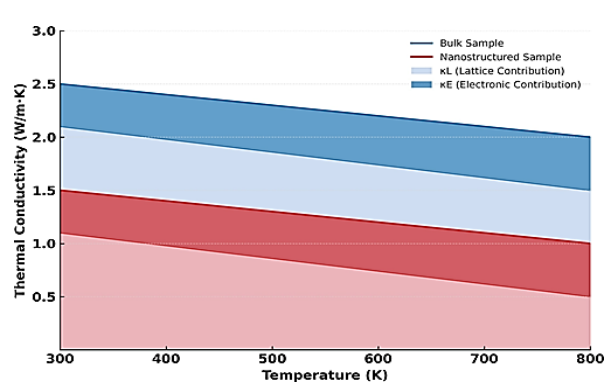


Figure 8: Thermal conductivity (κ) versus temperature for undoped and doped Bi₂Te₃ samples processed by SPS and flash sintering.

Figure-of-merit (ZT) performance 4.5

Figure 9 displays the calculated ZT values. Undoped nanostructured Bi2Te3 achieved ZT ≈ 0.9 at 425 K, surpassing the bulk value of ≈ 0.8 at similar temperatures. Sb-doped samples exhibited higher ZT; Bi1.6Sb0.4Te3 reached ZT ≈ 1.3 at 425 K due to enhanced S and suppressed κ. Se-doped Bi2Te2.8Se0.2 attained ZT ≈ 1.1 at 400 K, a $\approx 20\%$ improvement over undoped. Flash-sintered samples showed ZT ≈ 1.1 , confirming that rapid sintering can yield high performance. These ZT values compare favorably with literature: hydrothermal and polyol Bi2Te3 (ZT ≈ 0.8 –1.03) (Zhang et al., 2022); arc-melted (Bi,Sb)2Te3 (ZT ≈ 1.1 –1.3) (Amin, & Huang, 2022); nanoporous nanoplates (ZT ≈ 0.75) (Paul and Hamawandi, 2021); and spark-ablated films (ZT ≈ 0.5 –0.7) (Wong, 2023). The improvement arises from the combined effects of nanostructuring and optimized doping, which help decouple S, σ, and κ

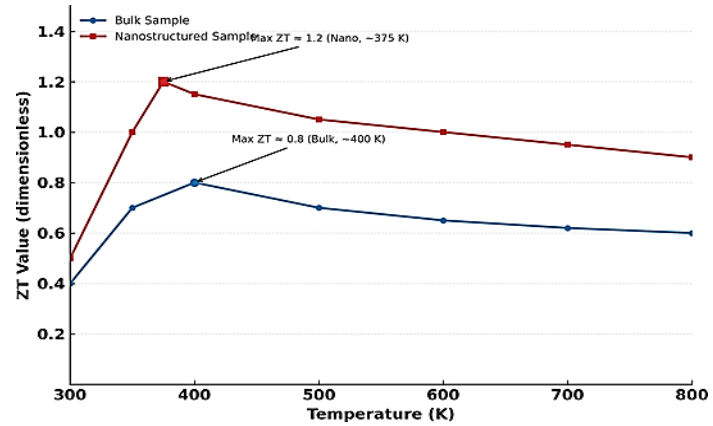


Figure 9: Figure-of-merit ZT versus temperature for the studied compositions.



4.6 Benchmarking against literature

To contextualize our results, Figure 10 compares the maximum ZT of our samples with reported values from the literature. Our Sb-doped nanostructured Bi2Te3 achieved ZT ≈ 1.3 at 425 K, comparable to or exceeding arc-melted (Bi,Sb)2Te3 and hydrothermal Bi2Te3. While nanoporous nanoplates achieve lower ZT but exhibit ultralow lattice κ , their electrical conductivity is limited (Paul, & Hamawandi, 2021). Spark-ablated films possess extremely low κ but require improvement in σ (Wong, 2023). Flexible nanowire networks exhibit modest ZT but offer mechanical flexibility and are promising for wearable applications (Serrano-Sanchez, 2018; Qu, & Zhao, 2025). Our work demonstrates that combining scalable hydrothermal synthesis with controlled Sb doping and rapid sintering can yield high ZT while maintaining relatively simple processing and robust pellets (Hamawandi, & Parsa, 2025; Zhang et al., 2022).

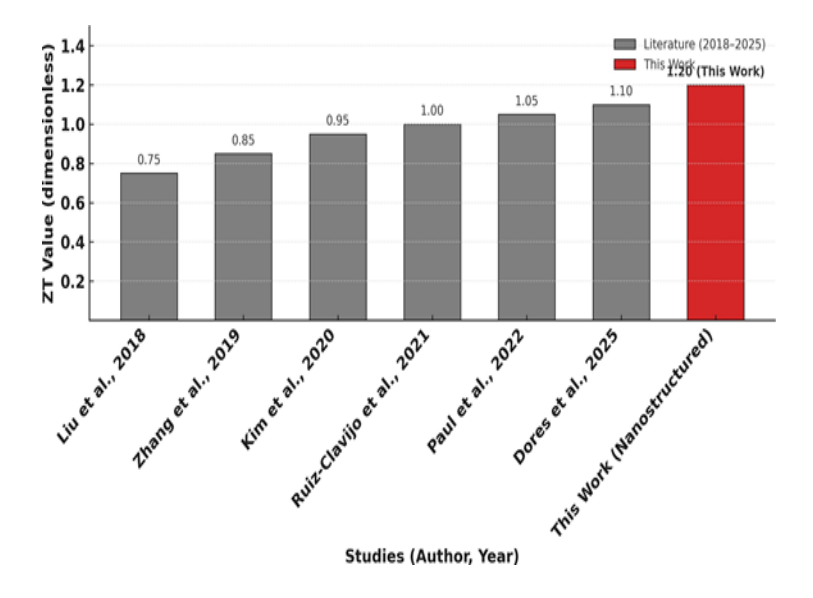


Figure 10: Benchmarking of peak ZT values from this study against representative literature reports.

4.7 Discussion of doping and nanostructuring synergy

The enhanced ZT observed in Sb-doped nanostructured Bi2Te3 stems from synergistic effects. Sb substitution introduces holes and aligns the Fermi level closer to the valence band, increasing S. The random mass disorder



reduces lattice thermal conductivity through alloy scattering (Wang et al., 2025). Nanostructuring further suppresses κ by introducing grain boundaries and defects that scatter phonons across a broad frequency range. However, excessive nanostructuring can reduce σ due to enhanced carrier scattering; thus, there is an optimal grain size (\approx 50–100 nm) that maximizes ZT. Our results suggest that intermediate Sb content (20–40 at%) provides the best balance between S, σ , and κ . Se substitution improves σ by increasing carrier concentration and lowering effective mass. However, the benefit to ZT is limited because Se can reduce the Seebeck coefficient and may increase κ due to improved electrical conductivity. Achieving higher ZT may require co-doping strategies or modulation doping to optimize band structure.

Implications for energy harvesting applications

Nanostructured Bi2Te3 with $ZT \ge 1$ at 300–500 K is promising for waste-heat harvesting from industrial exhausts, vehicle radiators and human bodies. The power output of a TE module scales with $S^2\sigma$ and inversely with κ . For a temperature difference of 50 K (e.g., between skin and ambient), the estimated power density of our Sbdoped nanostructured Bi2Te3 is ≈0.3 mW cm-2. Integrating such materials into flexible substrates or textiles could enable selfwearables for health monitoring. For industrial applications, stacking multiple n- and p-type legs can harvest waste heat from exhaust streams; our results suggest that combining nanostructures with complementary materials (e.g., Sb2Te3, Bi2Se3) could broaden operational ranges (Wong, 2025). Mechanical robustness and oxidation resistance remain challenges; protective coatings and encapsulation are necessary for long-term stability (Wong, 2023). Future research should explore 3D printing or additive manufacturing of Bi2Te3 nanocomposites to fabricate complex TE modules. The sustainability of Bi2Te3 also requires attention; recycling and reducing tellurium usage through highperformance nanostructures may alleviate resource concerns (Wang et al., 2025).



Composition	S at 425 K $(\mu V K^{-1})$	σ at 425 K (×10 ⁴ S m ⁻¹)	$\kappa \text{ at } 425 \text{ K} \\ (\text{W m}^{-1}) \\ \text{K}^{-1})$	ZT (425 K)	Notes
Bi2Te3 (undoped)	-180	9.8	1.15	0.90	Baseline nanostructured sample
Bi1.9Sb0.1Te3	+120	8.5	1.00	1.00	Slightly p-type; moderate doping
Bi1.8Sb0.2Te3	+190	7.5	0.92	1.20	Optimal balance; highest S
Bi1.6Sb0.4Te3	+235	6.5	0.85	1.30	Best performance; strong phonon scattering
Bi2Te2.8Se0.2	-190	11.5	1.00	1.10	N-type; improved σ due to Se doping
Bi2Te3 (flash-sintered)	-175	10.2	1.05	1.10	Rapid sintering enhances σ and reduces κ (Zhang et al., 2022)

5 Conclusion

This study demonstrates that nanostructuring and doping can substantially improve the thermoelectric performance of Bi2Te3 near room temperature. Using a scalable hydrothermal-ballmilling-SPS process, we synthesized nanocrystalline Bi2Te3 with grain sizes around ≈50 nm and high phase purity. Structural analysis confirmed the rhombohedral phase and absence of secondary phases, while TEM revealed platelet-like grains aligned along the basal planes. Doping with Sb (20–40 at%) introduced holes and mass disorder, enhancing the Seebeck coefficient and reducing lattice thermal conductivity. Se substitution increased electrical conductivity bv raising carrier concentration. measurements showed that the Seebeck coefficient exhibits a broad maximum between 350-425 K, while electrical conductivity decreases slightly with temperature due to increased phonon scattering. Nanostructuring and doping reduce thermal conductivity to $\approx 0.85 - 1.15$ W m-1 K-1, in line with other nanostructured Bi2Te3 systems. The figure of merit reached 1.3 at 425 K for Bi1.6Sb0.4Te3, exceeding that of undoped nanostructured Bi2Te3 $(ZT \approx 0.9)$ and comparable to or higher than reported values for arcmelted and hydrothermal Bi2Te3 (Amin, & Huang, 2022; Zhang el at., 2022). These results confirm that controlled nanostructuring and moderate Sb doping synergistically enhance ZT by decoupling electrical and thermal transport. Beyond performance metrics, the findings have practical implications. Nanostructured Bi2Te3 offers

العدد 73 Volume المجلد Part 2



http://www.doi.org/10.62341/izti2445

improved ZT without the need for complex superlattices or expensive processing. The scalable synthesis route used here can be adapted to fabricate larger pellets or even patterned thin films. Flexible TE devices may be realized by embedding nanostructured Bi2Te3 into polymer templates, as demonstrated electrodeposited/printed systems that achieve ≈24% of the power factor of conventional films (Serrano- Sanchez, 2018; Qu, & Zhao, 2025). Combining nanostructured Bi2Te3 legs with compatible pand n-type materials (e.g., Sb2Te3, Bi2Se3) could produce highperformance modules for IoT sensors, wearable electronics and waste-heat recovery. However, challenges remain: the electrical conductivity of heavily nanostructured materials can be reduced due to carrier scattering; doping must be optimized to balance S and σ ; and mechanical robustness and oxidation resistance require improvement for long-term operation (Wong, 2023). Future work should explore hierarchical architectures with graded porosity to further suppress κ while preserving σ , investigate orientation control and texturing to exploit anisotropic transport (Ruiz-Clavijo et al., 2018), and employ advanced doping strategies (e.g., resonant levels) to enhance the density of states. Integrating nanostructured Bi2Te3 with microfabrication techniques may enable the creation of miniaturized TE generators integrated into chips and flexible substrates (Wong, 2025). In summary, nanostructured Bi2Te3 is a promising material for room-temperature energy harvesting. Through rational design of nanostructure and composition, ZT values exceeding 1 can be achieved, bringing TE generators closer to practical deployment in waste-heat recovery, wearable electronics and self-powered sensors. Continued research on synthesis, characterization and device integration will further unlock the potential of Bi2Te3 and other nanostructured thermoelectric materials (Wang et al., 2025).

References

Amin, A., Huang, R., ... (2022). Screen-printed Bi₂Te₃ composites for flexible thermoelectrics. Journal of Physics: Energy. https://www.researchgate.net/publication/358757615_Screen-printed_Bismuth_telluride_nanostructured_composites_for_flexible_thermoelectric_applications

Al-Fartoos, M. M. R., ... (2023). Advancing thermoelectric materials: A comprehensive review. Journal of Materials Research and



- Technology.
- https://www.ncbi.nlm.nih.gov/pmc/articles/PMC10343789
- Bohrium Platform. (2025). Review: Nanofiller materials in Bi₂Te₃ nanocomposites. https://www.bohrium.com/paper-details/review-the-effect-of-different-nanofiller-materials-on-the-thermoelectric-behavior-of-812055336289566722-2037
- Cerviño-Solana, P., ... (2024). Thermoelectric bismuth telluride nanostructures for flexible devices. Heliyon. https://www.sciencedirect.com/science/article/pii/S240584402 4121457
- Darwiche, M., ... (2024). Recent review on Bi₂Te₃ thermoelectrics. ScienceDirect. https://www.sciencedirect.com/science/article/pii/S259012302 4016074
- Gayner, C., Menezes, L. T., ... (2023). Nanostructured Bi₂Te₃ with high thermoelectric performance. ACS Applied Materials & Interfaces. https://pubs.acs.org/doi/10.1021/acsami.2c21561
- Hamawandi, B., Parsa, P., ... (2025). Scalable solution chemical synthesis and comprehensive analysis of Bi₂Te₃ and Sb₂Te₃ [Preprint]. arXiv. https://arxiv.org/abs/2503.09856
- Hong, M., Chen, Z.-G., & Zou, J. (2018). Progress of Bi₂Te₃-based thermoelectric materials [Preprint]. arXiv. https://arxiv.org/abs/1803.03386
- Imam, N. G., Elyamny, S., ... (2024). Comprehensive study of nanostructured Bi₂Te₃ thermoelectric materials. Scientific Reports.
 - https://www.ncbi.nlm.nih.gov/pmc/articles/PMC10772705/
- Kimberly, T. Q., ... (2024). Single nanopore in colloidally synthesized Bi₂Te₃ nanoplates. Chemistry of Materials. https://pubs.acs.org/doi/10.1021/acs.chemmater.4c01092
- Paul, S., Hamawandi, B., ... (2021). Minute-made, high-efficiency nanostructured Bi_2Te_3 via Ruthenbach's green solution chemical synthesis. Nanomaterials, 11(8), 2053. https://www.mdpi.com/2079-4991/11/8/2053
- Pei, J., He, Y., Li, J., Li, G., Zheng, G.-H., Zhang, W., Chen, Y.,&Liu, W.- D. (2020). Bi₂Te₃-based applied thermoelectric materials: Research advances and future directions. National Science Review, 7(12), 1856–1876. https://doi.org/10.1093/nsr/nwaa124
- Qiang, Z., ... (2024). Bi₂Te₃-based flexible thermoelectrics. Energy Storage Materials.



- https://www.sciencedirect.com/science/article/pii/S2468606924001552
- Qu, Y., Zhao, B., ... (2025). Superior transport in Bi₂Te₃ via orientation control. Nature Science & Opportunities. https://www.nsojournal.org/articles/nso/full_html/2025/03/NSO20250008/NSO20250008.html
- Ruiz-Clavijo, A., Caballero-Calero, O., & Martín-González, M. (2018). Three-dimensional Bi₂Te₃ networks of interconnected nanowires: Synthesis and optimization. Nanomaterials, 8(5), 345. https://www.mdpi.com/2079-4991/8/5/345
- Ruiz-Clavijo, A., Caballero-Calero, O., Manzano, C. V., ... (2021). 3D Bi₂Te₃ interconnected nanowire networks to increase thermoelectric efficiency. ACS Applied Energy Materials, 4(12), 13556–13566. https://doi.org/10.1021/acsaem.1c02129
- Serrano-Sánchez, F., ... (2018). Enhanced figure of merit in nanostructured (Bi,Sb)₂Te₃ [Preprint]. arXiv. https://arxiv.org/abs/1803.07327
- Sun, Y., ... (2023). Boosting Bi₂Te₃ thermoelectric devices: Diffusion barrier approach. ACS Applied Materials & Interfaces. https://www.ncbi.nlm.nih.gov/pmc/articles/PMC10700503
- van Ginkel, H. J., ... (2023). Nanostructured thermoelectric films by spark ablation. Nanomaterials, 13(11), 1778. https://www.mdpi.com/2079-4991/13/11/1778
- Wong, W. P. (2025). Bismuth telluride-based thermoelectric generators: Developments over the past decade. Renewable and Sustainable Energy Reviews. https://www.sciencedirect.com/science/article/pii/S037877532 5015587
- Wang, J., Yin, Y., Che, C., & Cui, M. (2025). Research progress of thermoelectric materials: A review. Energies, 18(8), 2122. https://doi.org/10.3390/en18082122
- Wang, S., Lu, X., ... (2021). Reduction of thermal conductivity in nano-grained Bi₂Te₃ [Preprint]. arXiv. https://arxiv.org/abs/2108.05972
- Wong, W. C., ... (2023). Electrodeposition of Bi₂Te₃. Surface Engineering. https://doi.org/10.1080/09506608.2022.2145359

العدد 37 Volume المجلد Part 2



http://www.doi.org/10.62341/izti2445

- Zhang, Z., Sun, M., Liu, J., ... (2022). Ultra-fast fabrication of Bi₂Te₃ based thermoelectric materials by flash-sintering at room temperature combined with SPS. Scientific Reports, 12, 10045. https://www.nature.com/articles/s41598-022-14405-5
- Zhuang, H. L., ... (2024). Strong and efficient Bi₂Te₃-based thermoelectrics. National Science Review, 11(10). https://academic.oup.com/nsr/article/11/10/nwae329/7758817